Microchimica Acta
https://doi.org/10.1007/s00604-018-3112-z

ORIGINAL PAPER

Colorimetric determination of glucose in solution and via the use of a paper strip by exploiting the peroxidase and oxidase mimicking activity of bimetallic Cu-Pd nanoparticles deposited on reduced graphene oxide, graphitic carbon nitride, or MoS_2 nanosheets

Gitashree Darabdhara[1,2] · Purna K. Boruah[1,2] · Manash R. Das[1,2]

Received: 1 August 2018 / Accepted: 25 November 2018

Abstract
This work describes the preparation of bimetallic Cu-Pd nanoparticles (NPs) on supports like reduced graphene oxide (rGO), graphitic carbon nitride (g-C_3N_4) and MoS_2 sheets with a size of <10 nm. rGO is found to be the best support for synthesizing Cu-Pd NPs with controlled shape, size and oxidation state. The Cu-Pd/rGO nanocomposite also demonstrated the best peroxidase and oxidase mimicking activity compared to Cu-Pd/g-C_3N_4 and Cu-Pd/MoS_2 nanocomposites. The peroxidase mimicking activity of Cu-Pd/rGO was investigated in more detail, and a glucose oxidase (GOx) based glucose sensor was constructed that is based on the enzymatic formation of H_2O_2 and the Cu-Pd NPs-assisted oxidation of tetramethylbenzidine by H_2O_2 to give a blue-green coloration with absorption maxima at 652 nm. The assay has a 0.29 μM detection limit and a detection range that extends from 0.2 to 50 μM. The method was applied to the determination of glucose in diluted serum samples, and results compared well to those acquired with a clinical analyzer. The method also was applied in a colorimetric paper-based test stripe that can detect glucose within 10 min.

Keywords 2D nanosheets · 3,3′,5,5′-Tetramethylbenzidine · Colorimetric assay · Glucose assay · Paper device · Enzyme mimic

Introduction

Nanomaterials composed of metals [1], metal oxides and sulphide [2, 3] and carbon based nanostructures [4] can exhibit oxidase, peroxidase, catalase or superoxide dismutase mimetic activity. Bimetallic nanoparticles, a class of materials offering synergistic effects via cooperative interactions resulting in enhanced catalytic activity, promoted electron transfer, biocompatibility and increased surface area than the corresponding monometallic systems [5]. Bimetallic nanozymes like Au-Pd bimetallic nanocomposites [6], core-shell Au-Pd/MoS_2 [7], Pt-Ag NPs on ultrathin MoS_2 [8] etc. as efficient peroxidase mimics has been explored. Considering the multi-enzyme mimic activity and excellent catalytic properties, noble metals like Pd, Pt and Au with transition metals, metal oxides and carbon materials have been widely investigated. Nanomaterials of Pd are worth mentioning as they behave as promising enzyme mimics and are extensively used in biological detection, immunoassay etc. However, its high cost persuades researchers to fabricate bimetallic Pd catalyst with low cost transition metals capable of rendering improved activity via modification of the structural and electronic properties of the active catalytic sites [9]. In this respect, Cu which is cheaper and possess high natural abundance is widely applicable as a catalyst [10], sensor [11], in biomedicine [12] and can be a good alloying partner for Pd. Theoretical studies have triggered increasing interest in the nano alloys

Electronic supplementary material The online version of this article (https://doi.org/10.1007/s00604-018-3112-z) contains supplementary material, which is available to authorized users.

✉ Manash R. Das
mnshrdas@yahoo.com; mrdas@neist.res.in

[1] Advanced Materials Group, Materials Sciences and Technology Division, CSIR-North East Institute of Science and Technology, Jorhat, Assam 785006, India

[2] Academy of Scientific and Innovative Research, CSIR - Human Resource Development Centre, Ghaziabad, Uttar Pradesh 201002, India

Published online: 11 December 2018

of Pd and Cu which acts as highly active catalyst in the CO oxidation [13], oxygen reduction reaction [14], reduction of nitroaromatics and hexavalent chromium [15] etc. Considering the superior activity of Cu-Pd alloy nanoparticles in different reactions and the noteworthy contribution of individual Pd and Cu as artificial enzymes, it is expected that the Cu-Pd alloy system can behave as superior intrinsic enzyme mimetics.

Improving the nanoparticles' physical and chemical properties via interaction with a support material is another subject of profound interest. Two-dimensional (2D) nanomaterials possessing sheet like structures are an emerging class of nanomaterials whose renaissance is marked with the discovery of graphene in 2004 [16]. Graphene, a one atom thick sp^2 hybridized carbon atom exhibits exceptional properties and acts as excellent support for anchoring metal nanoparticles. A number of monometallic and bimetallic nanoparticles like Au, Ag, Pd, Au-Pd, Pd-Ru etc. have been synthesized on graphene exhibiting significant catalytic properties [17]. These sensational properties revitalized work on other 2D materials like graphitic carbon nitride (g-C_3N_4) [18], transitional metal dichalcogenides (TMDs) [19] etc. g-C_3N_4 and MoS_2 nanosheets are amongst emerging 2D materials finding application in numerous areas. g-C_3N_4 is environment friendly, inexpensive and possesses appreciable thermal and chemical stability, tunable electronic structure [20], high fluorescence quantum yield and biocompatibility. MoS_2, a lamellar structured TMD is an attracting material with widespread application in catalysis [21], energy storage [22] etc. Thus, developing Cu-Pd nanoparticles on such fascinating 2D support would significantly enhance the properties of individual Cu, Pd and the 2D support as well as add newer properties to the nanocomposite and is expected to behave as good enzyme mimicking nanomaterial.

Nanoparticles exhibiting peroxidase activity are capable of catalyzing 3,3′,5,5′-tetramethylbenzidine (TMB) in presence of H_2O_2 to blue colored 3,3′,5,5′-tetramethylbenzidine diimine (TMBDI) exhibiting an absorbance maxima at 652 nm. This less cost effective colorimetric assay can be utilized as a podium for the detection of molecules like glucose [23]. Glucose is indispensable in life cycles and alterations in its level cause's disorders of kidneys, heart, etc. [24]. Thus, detecting glucose concentration in real time is mandatory. Paper based analytical devices, a class of disposable devices possessing the benefits of self pumping, low cost and availability has drawn attraction in microfluidic research on the development of biosensors and electronic applications for the point of care diagnostics [25].

This work demonstrates the synthesis of Cu-Pd nanoparticles on 2D sheets namely reduced graphene oxide (rGO), g-C_3N_4 and MoS_2 demonstrating enzymatic peroxidase and oxidase like behavior. Amongst all the nanocomposites, Cu-Pd/rGO exhibited excellent and higher peroxidase activity for oxidation of TMB, 2,2′-azino-bis(3-ethylbenzo-thiazoline-6-sulfonic acid) diammonium salt (ABTS) and o-phenylenediamine (OPD) in presence of H_2O_2. Additionally, Cu-Pd/rGO exhibited oxidase like activity capable of oxidizing TMB in absence of H_2O_2. A colorimetric glucose detection assay was reported based on the colour change of TMB with the catalytic reaction of glucose with glucose oxidase (GOx). Furthermore, a portable paper based analytical device embedded with the Cu-Pd/rGO nanocomposite was designed for the point of care diagnosis of glucose.

Experimental

Materials

Details on materials is provided in the Electronic Supplementary Material (ESM).

Synthesis of GO, g-C_3N_4 and MoS_2 nanosheets

Graphite oxide was synthesized by Hummers and Offemann's method followed by ultrasonication to obtain graphene oxide (GO) sheets [26].

For 2D g-C_3N_4, urea (15 g) was calcinated at 550 °C for 3 h at 5 °C min^{-1} to obtain a yellow product which was ultrasonicated in water to obtain g-C_3N_4 nanosheets (10 mg mL^{-1}).

For MoS_2 nanosheets, sodium molybdate (0.62 g) and thiourea (2.74 g) was mixed in water and transferred to a autoclave and heated at 200 °C for 12 h. Resulting solid was collected and dispersed in water to obtain MoS_2 sheets (10 mg mL^{-1}).

Preparation of Cu-Pd/rGO, Cu-Pd/g-C_3N_4 and Cu-Pd/MoS_2 nanocomposites

For Cu-Pd/rGO nanocomposites, $Cu(CH_3COO)_2.H_2O$ (23.9 mg) and $PdCl_2$ (21.2 mg) was dissolved in 16 mL H_2O in 1:1 millimolar ratio followed by the addition of 10 mL of GO (10 mg mL^{-1}). To the reaction mixture trisodium citrate, 20.6 mg dissolved in 7 mL H_2O was added dropwise followed by addition of ascorbic acid, 70.4 mg in 7 mL H_2O and heated at 80 °C for 3 h. The solid product was washed with water and ethanol five times and dried to obtain Cu-Pd/rGO nanocomposite. Three different Cu-Pd/rGO nanocomposites were synthesized where millimolar ratios of precursors $Cu(CH_3COO)_2.H_2O$ and $PdCl_2$ were 1:1, 1:2 and 2:1 and designated as Cu-Pd 1/rGO, Cu-Pd 2/rGO and Cu-Pd 3/rGO, respectively. Monometallic Cu/rGO and Pd/rGO were synthesized adopting similar procedures by mixing either

$Cu(CH_3COO)_2.H_2O$ or $PdCl_2$ with GO to obtain Cu/rGO and Pd/rGO, respectively.

Likewise, nanocomposites of g-C_3N_4 and MoS_2 were synthesized replacing GO with g-C_3N_4 and MoS_2 to form Cu-Pd/g-C_3N_4 and Cu-Pd/MoS_2 nanocomposites, respectively. The Cu-Pd/g-C_3N_4 and Cu-Pd/MoS_2 nanocomposites were synthesized using 1:1 millimolar ratios of precursors $Cu(CH_3COO)_2.H_2O$ and $PdCl_2$.

Instrumental techniques

Details instrumental techniques are provided in the ESM.

Peroxidase like activity

The peroxidase like activity was investigated through the catalytic oxidation of TMB, ABTS and OPD in presence of H_2O_2. To a 3.5 mL sodium acetate buffer (pH 4), 0.250 mL of 0.01 M TMB, 0.05 mL of 100 mM H_2O_2 and 0.025 mL of Cu-Pd/rGO nanocomposite (1 mg mL^{-1}) was added and incubated for 10 min followed by monitoring the absorbance at 652 nm by a UV-visible spectrophotometer. Parameters like effect of different catalysts, catalyst concentration (1 mg mL^{-1} –12 mg mL^{-1}), pH (2 to 9) and temperature (25 °C – 55 °C) were analyzed. Kinetics analysis was carried out by changing the concentration of either TMB (0.02–10 mM) or H_2O_2 (10–400 mM) at a time and keeping the other constant. The absorbance data were converted to concentration values using the Beer–Lambert law with a molar absorption coefficient of 39,000 M^{-1} cm^{-1} at 652 nm for TMB–derived oxidation products. Typical Michaelis-Menten curves and corresponding Lineweaver-Burk double reciprocal plot gives the value of Michaelis constant (K_m) and maximum rate of conversion (V_{max}) on the basis of the following equation

$$\frac{1}{v} = \left(\frac{Km}{Vmax}\right)\left(\frac{1}{[S]}\right) + \left(\frac{1}{Vmax}\right) \quad (1)$$

Glucose detection in standard and real samples

0.1 mL of 10 mg·mL^{-1} glucose oxidase (GOx) and 0.1 mL of glucose at different concentrations (1 μM–1 mM) in phosphate buffer solution (10 mM, pH 7.0) was incubated at 37 °C for 30 min. This was followed by addition of 0.3 mL of 20 mM TMB, 0.05 mL of Cu-Pd/rGO (7 mg mL^{-1}) and 2.5 mL sodium acetate buffer (pH 4). The entire solution was incubated for 10 min at 35 °C and the absorbance at 652 nm was noted to prepare the standard calibration plot for glucose. The selectivity of this process was analyzed against glucose analogues maltose, fructose, lactose, dopamine; L-cysteine and ascorbic acid in a similar way but the concentration of all other molecules were 10 times stronger than glucose. For real sample analysis, blood serum were collected from human volunteers from CSIR-NEIST Jorhat, Assam, India and centrifuged at 4000 rpm for 5 min. The collected supernatants were diluted twenty times using phosphate buffer solution and used for further measurements. The absorbance at 652 nm was then monitored using UV–vis spectrophotometry.

Construction of a paper analytical device for glucose detection

Filter paper was cut in the shape of a straight strip of length 30 mm and width 6 mm possessing a circular head of 10 mm. The strips were washed with hot DI water and coated with 0.5% polyvinyl alcohol (PVA). They were further coated with 0.2 mL of Cu-Pd/rGO nanocomposite (7 mg mL^{-1}) followed by administration of GOx solution (100 μL of 10 mg mL^{-1}) and then allowed to dry at 45 °C for 2 h in an air oven. After drying, the circular heads were drop casted with freshly prepared TMB (0.3 mL) and dried at room temperature. Next, the feet of the paper were kept vertically in different petridishes so that the paper remains immersed in glucose solutions of different concentrations (1–100 μM). The glucose solutions moved up the paper due to capillary action and reached the circular head within moments and oxidation of TMB was immediately initiated resulting in production of blue colour due to formation of TMBDI exhibiting absorbance maxima at 652 nm. Depending upon the concentration of glucose present the colour change on the head of the paper differs.

Results and discussions

Characterization of Cu-Pd/rGO, Cu-Pd/g-C_3N_4 and Cu-Pd/MoS_2 nanocomposites

Figure 1a shows the TEM images of the Cu-Pd/rGO nanocomposites. The TEM images of the Cu-Pd 1/rGO nanocomposites (Fig. 1a (a-c)) shows well dispersed spherical Cu-Pd nanoparticles on the rGO layers with a narrow size distribution. HRTEM images of the Cu-Pd 1/rGO (Fig. 1a(b)) shows the multi-phase structure with distinct interplanar spacing of 0.224 nm corresponding to *fcc* (111) plane of Pd and 0.201 nm consistent with the (111) plane of *fcc* Cu. The average particle size processed using Image J software from a population of 80 particles is found to be 4.36 ± 0.16 nm (Fig. 1a(c)). The TEM image of Cu-Pd 2/rGO nanocomposites (Fig. 1a(d)) shows agglomeration resulting from the increased Pd concentration. The HRTEM image of the Cu-Pd 2/rGO nanocomposites (Fig. 1a(e)) displays two different lattice fringes corresponding to the (111) plane of Cu and Pd in a single nanoparticles with an average size of 6.58 ± 0.31 nm calculated from a population of 50 particles. The TEM images of Cu-Pd 3/rGO nanocomposites displays similar results with an average size of 5.74 ±

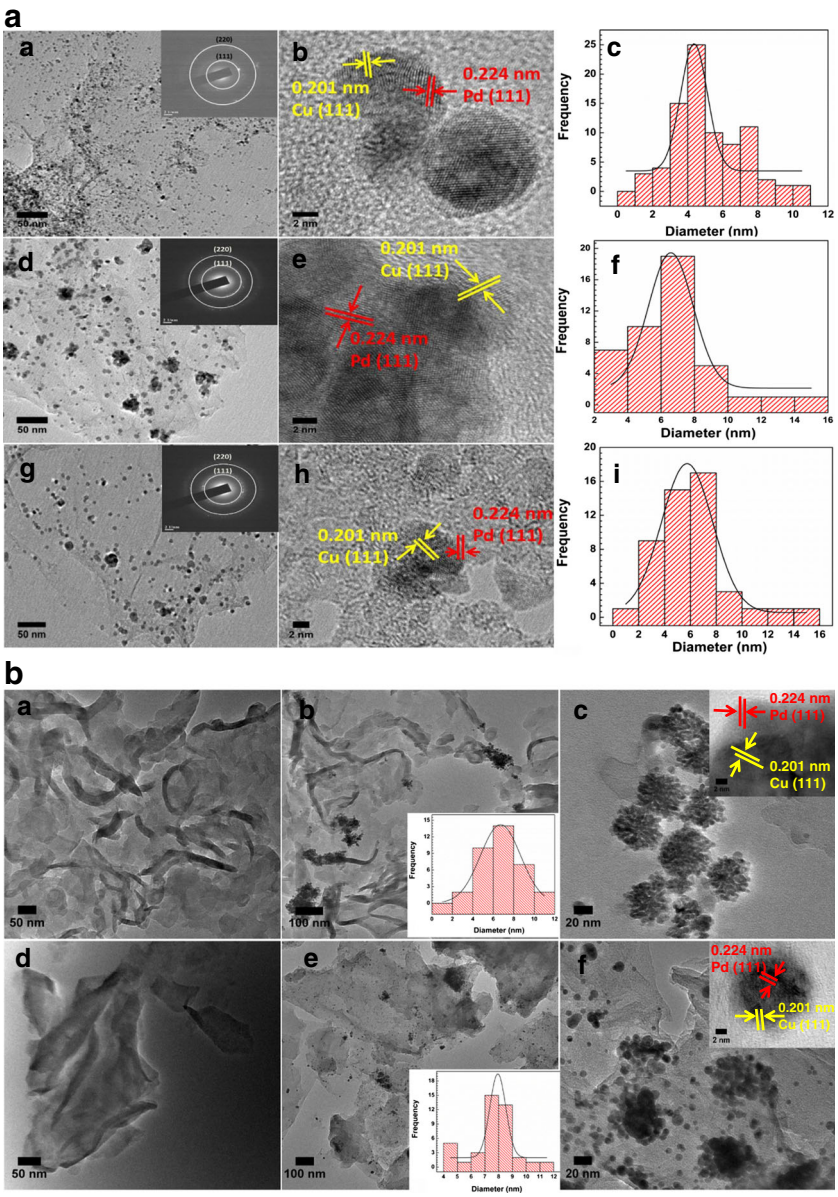

Fig. 1 **a** TEM image (a), HRTEM (b), size distribution histogram (c) of Cu-Pd 1/rGO; TEM image (d), HRTEM (e), size distribution histogram, (f) of Cu-Pd 2/rGO; TEM image (g), HRTEM (h), size distribution histogram (i) of Cu-Pd 3/rGO nanocomposites; **b** TEM image of g-C_3N_4 nanosheets (a), Cu-Pd/g-C_3N_4 nanocomposites (b, c), MoS_2 nanosheets (d), Cu-Pd/MoS_2 nanocomposites (e, f). Insets (b, e) shows the size distribution histogram and (c, f) shows the corresponding HRTEM images

0.24 nm calculated from a population of 55 particles (Fig. 1a(g-h)). The Cu-Pd nanoparticles synthesized using 1:1 ratios of the metal precursors resulted in alloy nanoparticles of the smallest size and well distribution. Further analysis on the morphology of the Cu-Pd 1/rGO nanocomposites was studied using high-angle annular dark-field scanning transmission electron microscopy (HAADF-STEM) and elemental mapping images as shown in Fig. S1. This confirms the presence of both Cu and Pd highly dispersed on the rGO surface. The TEM images of monometallic Cu/rGO and Pd/rGO are provided in Fig. S2 and discussed.

The TEM image of g-C_3N_4 (Fig. 1b (a)) exhibits layered structure comprising of small sheets with wrinkles. The TEM image of Cu-Pd/g-C_3N_4 nanocomposites (Fig. 1b (b)) shows the presence Cu-Pd nanoparticles on g-C_3N_4 nanosheets with a heterogeneous distribution and average particle size of 6.7 ± 0.09 nm calculated from a population of 52 particles. They are also observed to be agglomerated in several areas. Fig. 1b (c) reveals flower like aggregates of Cu-Pd nanoparticles on g-C_3N_4 nanosheets and the HRTEM image (Fig. 1b (c) inset) clearly depicts the presence of lattice fringes corresponding to the *fcc* Cu (111) and Pd (111) planes. The sheet like morphology of the MoS_2 is also evident from Fig. 1b (d). The morphology of the Cu-Pd/MoS_2 (Fig. 1b(e,f)) shows that the Cu-Pd nanoparticles are non-uniformly dispersed on MoS_2 nanosheets forming the assembly of MoS_2 nanosheets and Cu-Pd spherical nanostructures. The average size is found to be 7.94 ± 0.07 nm calculated from a population of 48 particles. Fig. 1b

(f) reveals that the Cu-Pd nanoparticles have undergone agglomeration over the MoS_2 surface and the HRTEM image (Fig. 1b (f) inset) confirms the presence of both Cu and Pd lattice fringes. A comparison of the TEM analysis of the Cu-Pd nanoparticles synthesized on different supports shows that rGO acted as a better support for dispersing smallest size Cu-Pd nanoparticles homogeneously on its surface without considerable agglomeration. However, both Cu-Pd/g-C_3N_4 and Cu-Pd/MoS_2 nanocomposites underwent considerable agglomeration with non-uniform distribution. TEM characterization thus clearly suggests that rGO behaves as a better support than both g-C_3N_4 and MoS_2 for synthesizing Cu-Pd nanoparticles with smaller size and homogenous distribution.

Study on the chemical composition and the oxidation states of all the nanocomposites were carried out using XPS analysis. The low resolution XPS survey spectrum of all the nanocomposites is shown in Fig. S3 which displays prominent peaks corresponding to C1s (284.97 eV), O1s (533 eV), Pd3d (336.18 eV) and Cu2p (932.41 eV) for Cu-Pd/rGO; C1s (284.96 eV), N1 s (396.21 eV), Pd3d (335.25 eV) and Cu2p (934.34 eV) for Cu-Pd/g-C_3N_4; Mo3d (232.31 eV), S2p (168.34 eV), Pd3d (336.37 eV) and Cu2p (935.58 eV) for Cu-Pd/MoS_2 nanocomposites, respectively and their chemical composition is provided in Table S1. The high resolution XPS spectra for Cu-Pd/rGO along with monometallic Cu/rGO and Pd/rGO are provided in details in the ESM (Fig. S4 and S5, respectively) along with the XPS of Cu-Pd/g-C_3N_4 and Cu-Pd/MoS_2 in Fig. S6. From the XPS analysis it is evident that both Cu and Pd are present in (0) oxidation states in Cu-Pd/rGO nanocomposite whereas they went substantial oxidation when synthesized on g-C_3N_4 and MoS_2 nanosheets to form Cu-Pd/g-C_3N_4 and Cu-Pd/MoS_2 nanocomposites. Detailed characterizations using other techniques like XRD, FESEM, DRIFT and TGA are furnished in the ESM from Fig. S7–S11.

Enzyme like catalytic activity

Peroxidase like catalytic activity of the nanocomposites was evaluated for TMB oxidation in presence of H_2O_2 for 10 min (Fig. 2a). All the catalyst effectively oxidizes TMB to blue colour TMBDI exhibiting absorbance maxima at 652 nm. The peroxidase activity of the catalysts follows the order Cu-Pd 1/rGO > Cu-Pd 2/rGO > Cu-Pd 3/rGO > Cu-Pd/g-C_3N_4 > Cu-Pd/MoS_2 > Cu/rGO > Pd/rGO. The results confirmed that bimetallic Cu-Pd alloy nanoparticles synthesized in 1:1 millimolar ratio of the metal precursors and supported on rGO exhibited highest peroxidase activity was thus used for carrying out further enzyme catalytic activity. The high catalytic activity of Cu-Pd/rGO compared to Cu-Pd/g-C_3N_4 and Cu-Pd/MoS_2 nanocomposites is due to the small size and well distribution of the nanoparticles as confirmed from TEM analysis. This leads to increased surface area and high catalytic sites in Cu-Pd/rGO for the adsorption of TMB molecules. Moreover both Cu and Pd in Cu-Pd/rGO nanocomposite are present in (0) oxidation states and are thus stable in nature. On the other hand the Cu-Pd nanoparticles supported on g-C_3N_4 and MoS_2 nanosheets are heterogeneously distributed and are agglomerated in several areas. Additionally they possess larger size than Cu-Pd/rGO nanocomposite which leads to decreased catalytic sites and hence lowered activity. Also, rGO possess a large number of π electrons that can be transferred to the bimetallic center creating a good network for electron mobilization and easy adsorption by TMB. The amino groups present on the TMB offers many lone electron pairs that could pass the electrons to the nanocomposites and thus provide easy access of electrons to reduce H_2O_2. H_2O_2 gets converted to H_2O and consequently rate of TMB oxidation increases. These factors contribute towards the high performance of Cu-Pd/rGO nanocomposite to peroxidase mimicking activity.

The oxidation of TMB was also evaluated using Cu-Pd 1/rGO catalytic system more commonly referred to as Cu-Pd/rGO under different conditions as shown in Fig. 2b. From the figure it is observed that both H_2O_2 and Cu-Pd/rGO nanocomposite is required for efficient oxidation of TMB. The catalyst with the best activity was further selected to examine its ability to test the oxidation of other substrates like ABTS and OPD. Cu-Pd/rGO is capable of catalyzing fast oxidation of TMB, ABTS and OPD in presence of H_2O_2 to give different colored solutions and typical absorption curves are shown in Fig. 3a. At the same time the Cu-Pd/rGO nanocomposites also catalyzes the direct oxidation of TMB in absence of H_2O_2 suggesting the oxidase like behavior of Cu-Pd/rGO nanocomposites (Fig. 3b). Thus, in conclusion, Cu-Pd/rGO nanocomposites exhibited dual enzyme mimetic activity. The TMB oxidation reaction was carried out further using Cu-Pd/rGO nanocomposite to analyze the dependence on pH, temperature and catalyst loading as shown in Fig. S12. It is found that the TMB oxidation was most effective at pH 4, with a 7 mg L^{-1} catalyst loading amount at 35 °C.

Kinetic studies of peroxidase like activity

Steady state kinetics was investigated using Cu-Pd/rGO under optimal reaction conditions (pH 4, 7 mg L^{-1} Cu-Pd/rGO and 35 °C) using H_2O_2 and TMB as substrates and by changing the concentration of one substrate at a time while keeping the other constant. A series of experiments were carried out and the Michaelis Menten curves were found by changing the absorbance values to their corresponding concentration using the Beer Lambert's law:

$$A = \varepsilon_{TMBDI} \times c \times L \quad (2)$$

Where, ε_{TMBDI} = 39,000 M^{-1} cm^{-1} for TMB.

Fig. S13 (a) shows the Michaelis Menten kinetics for TMB and H_2O_2. K_m and V_{max} of the Cu-Pd/rGO enzyme mimic was

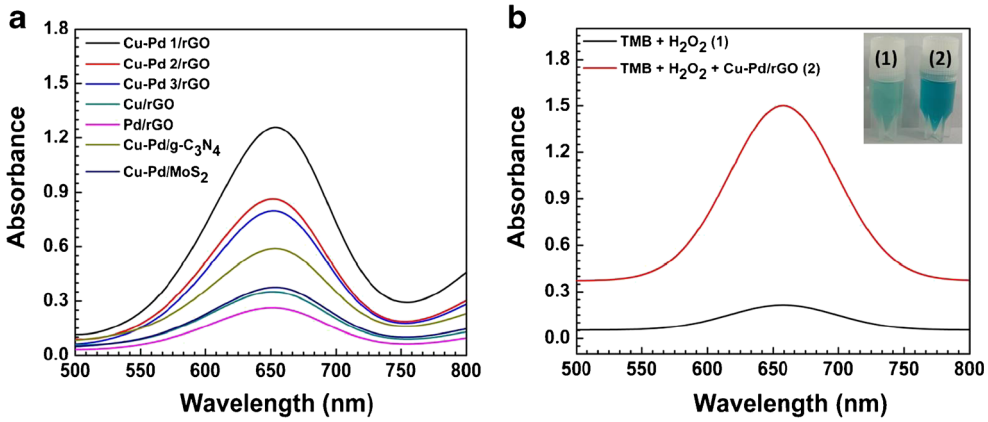

Fig. 2 **a** UV-visible curves showing TMB oxidation as a function of different catalyst (**b**) Absorbance spectra of TMB in presence of H_2O_2 alone and in presence of both H_2O_2 and Cu-Pd/rGO nanocomposite

calculated from the Lineweaver Burk plots (Fig. S13 a, b insets) where the intercept gives V_{max} and the slope gives K_m. The kinetics parameters were calculated and summarized in Table S2. All the experiments were carried out in duplicate. The K_m value (0.211 mM for TMB) exhibited by Cu-Pd/rGO was found to be lower than horseradish peroxidase (HRP, 0.434 mM) indicating higher substrate affinity of Cu-Pd/rGO than HRP. Moreover, the K_m value was found to be lower than the monometallic analogues as well as Cu-Pd/g-C_3N_4 and Cu-Pd/MoS_2 nanocomposites towards TMB. The K_m value for Cu-Pd/rGO with TMB as well as H_2O_2 is much lower which indicates better efficiency of this material and the fact that lower H_2O_2 concentration is required for TMB oxidation.

Determination of glucose and selectivity study

Considering the enzyme mimic property of the Cu-Pd/rGO nanocomposite, a colorimetric platform was designed for glucose detection using TMB. As H_2O_2 is the main product of the glucose catalytic reaction by GOx, the TMB-H_2O_2 reaction couples with the glucose reaction to produce the blue colored oxidized TMBDI exhibiting maximum absorbance at 652 nm. GOx in presence of oxygen catalyzes the conversion of glucose to gluconic acid and H_2O_2 and the released H_2O_2 catalyzed by Cu-Pd/rGO reacts with TMB to produce TMBDI. The colour change from the converted TMB is then employed for determining the glucose content. The calibration plot for standard glucose detection is shown in Fig. 4a with a linear detection range between 0.2 and 50 μM and limit of detection 0.29 μM. The selectivity for the process was studied considering lactose, maltose, fructose, dopamine, L-cysteine and ascorbic acid (Fig. 4b) which shows the better selectivity of Cu-Pd/rGO nanocomposites towards glucose. All the experiments were carried out in duplicate. Comparative table for glucose detection using other reported enzyme mimics is presented in Table 1 [8, 27–30]. It is seen that the catalytic activity of our synthesized Cu-Pd/rGO nanozyme is comparative to many other reported nanozymes and in certain cases are even better. The work reported by Nirala et al. on the peroxidase activity of nanoporous palladium (II) bridged coordination polymer outperforms the activity of our nanozyme in terms of detection limit of 0.047 μM and range of glucose detection, 1–300 μM [29]. However, their enzyme could exhibit only peroxidase like activity whereas Cu-Pd/rGO nanocomposite exhibited both peroxidase and oxidase like catalytic activity and is also capable of oxidizing other peroxidase substrates such as OPD and ABTS along with TMB. Moreover, our nanozyme system could be repeatedly reused upto five cycles without much loss in its activity which is discussed in the next section. Thus, our designed biosensor is reusable and sustainable in nature which implies its utility in robust practical fields.

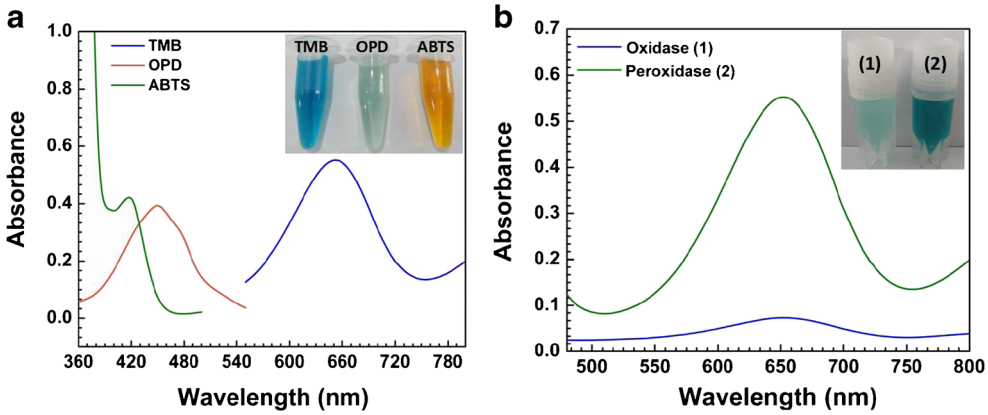

Fig. 3 **a** UV-visible spectra showing oxidation of TMB, OPD and ABTS using Cu-Pd/rGO nanocomposite (**b**) Oxidase like activity of Cu-Pd/rGO nanocomposite

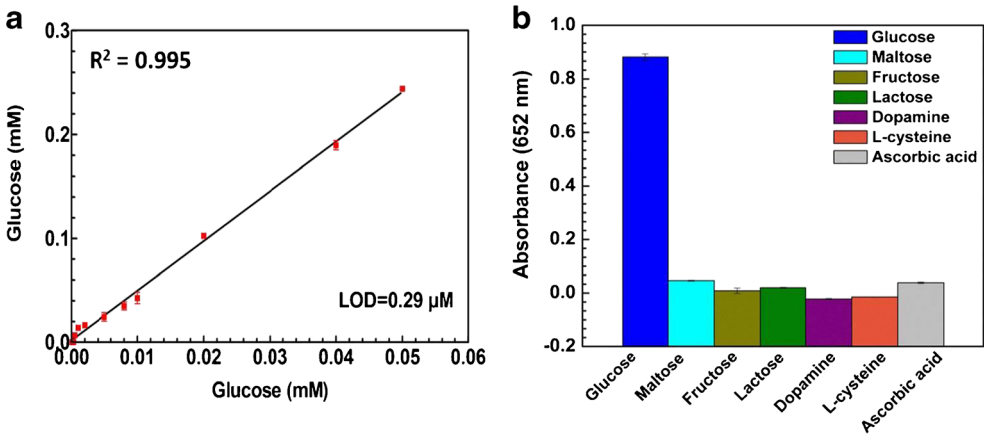

Fig. 4 **a** Standard calibration plot of glucose using Cu-Pd/rGO nanocomposite (**b**) Selectivity study of TMB oxidation in presence of different glucose analogues

Glucose detection mechanism

The origin of glucose catalytic reaction is the generation of hydroxyl radical (OH ·) from the decomposition of H_2O_2 as shown in following steps:

$$O_2 + \text{Glucose} \xrightarrow{\text{GOx}} H_2O_2 + \text{Gluconic acid} \quad (3)$$

$$H_2O_2 \longrightarrow OH\cdot \quad (4)$$

$$\text{TMB (colorless)} + OH\cdot \xrightarrow{\text{Cu–Pd/rGO}} \text{TMBDI (blue)} + H_2O \quad (5)$$

In presence of O_2 and GOx, glucose is oxidized to gluconic acid along with release in H_2O_2 (Eq. 3) which gets adsorbed over the Cu-Pd/rGO nanocomposite surface and via Fenton type reaction generates OH· radical (Eq. 4). The formed OH· radical quantitatively oxidizes TMB present in the reaction to the corresponding TMBDI (Eq. 5). The generation of OH· radical was assessed by adding a fluorescent probe terephthalic acid (TA) which reacts with OH· to produce fluorescent 2-hydroxyterepthalic acid [31]. Original TA do not exhibit fluorescence under excitation but glucose-GOx/TA system in presence of Cu-Pd/rGO exhibits considerable fluorescence ~420 nm when excited at 315 nm (Fig. S14). The glucose- GOx/TA system in absence of Cu-Pd/rGO do not exhibit significant fluorescence signal thus suggesting that Cu-Pd/rGO nanocomposites can decompose in-situ formation of H_2O_2 from glucose-GOx system to produce OH· radical.

Glucose detection in real samples

The glucose determination technique can be extended to estimate glucose in real samples like blood serum of human volunteers as shown in Fig. S15. The glucose concentration determined in blood serum from the standard glucose calibration plot was found to be 5.89 and 4.74 mM. The glucose concentration determined using our method agrees to that determined using standard hospital method and is presented in Table S3 and thus we can successfully utilize our method to determine glucose concentration in real samples.

Construction of paper based analytical device

To make the detection process more user friendly we extended the concept towards construction of a paper based analytical device. A filter paper was used and the process for construction of the paper strips is described in the Experimental Section. The surface morphology of the paper strips were studied using FESEM. The morphology of the paper before PVA coating shows the porous structure of cellulose (Fig. S16 (a, b)) which decrease after being coated with 0.5% PVA solution (Fig. S16 (c, d)). PVA coating has no effect on the morphology and porosity of the paper and also helps to retain aqueous samples which have an affinity to spread on normal paper. The FESEM images of Cu-Pd/rGO nanocomposites coated paper strips clearly show the presence of spherical Cu-Pd/rGO nanocomposites on the

Table 1 Comparison of colorimetric methods for determination of glucose using peroxidase mimics

Catalyst	Linear Range	Limit of detection	Ref.
Bimetallic Bi/Pt	1–100 μM	0.2 μM	[27]
3D graphene/Fe_3O_4 – AuNPs	0.02–0.19 μM	0.012 μM	[28]
MoS_2-$Pt_{74}Ag_{26}$ nanohybrids	5–150 μM	1.2 μM	[8]
Nanoporous palladium(II) bridged coordination polymer	1–300 μM	0.047 μM	[29]
FeOOH/N-doped carbon nanosheets	0.08 μM −0.8 mM	0.2 μM	[30]
Cu-Pd/rGO nanocomposites	0.5 and 50 μM	0.29 μM	This work

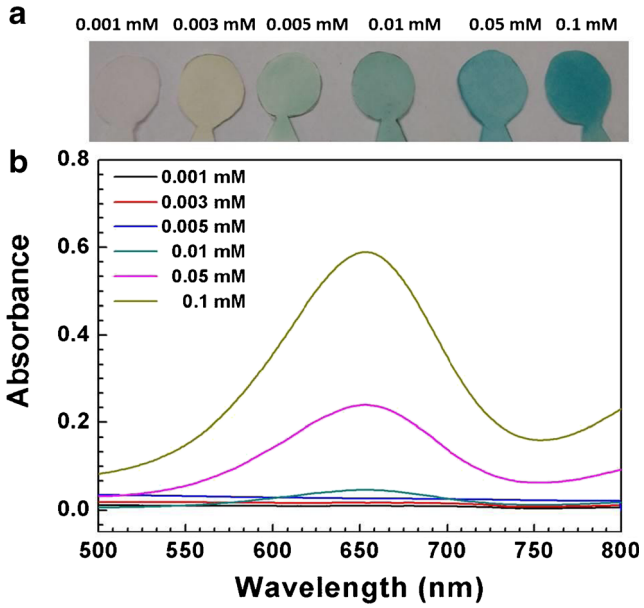

Fig. 5 **a** Paper strip assay of Cu-Pd/rGO nanosensor using glucose of varying concentration (**b** UV-visible spectra of the paper strips dipped in different glucose solutions

paper matrix (Fig. S17 (a-c)). The porous nature of the cellulose was completely coated with Cu-Pd/rGO nanocomposites and the EDX analysis confirms the presence of Cu and Pd on the paper matrix (Fig. S17 d).

The head of the constructed paper strips after being coated with nanocomposites were drop casted with freshly prepared TMB and the feet of the paper was allowed to stand in glucose solutions of varying concentrations. The glucose solutions move up to the circular head of the paper strip via capillary action and resulted in immediate colour change after interaction with TMB their in. Depending upon the glucose concentration, the oxidation of TMB and the colour generation varies and as shown in Fig. 5a. The results were confirmed by performing the solid state UV-visible analysis of the paper strips as shown in Fig. 5b and maximum absorbance is noted for the glucose solution with highest concentration. The colour change is significant and can be detected using bare eyes and thus this study suggests that such types of user friendly paper strip devices can be easily implemented for fast and ready detection of glucose.

Reusability and sustainability of the Cu-Pd/rGO nanocomposites

Recyclability of the Cu-Pd/rGO was studied upto five cycles. After each cycle, the catalyst was separated, washed with hot water followed by acetone and dried in a hot oven followed by mixing with freshly prepared TMB to study the oxidized product. Figure 6a shows that the intensity of TMB oxidation

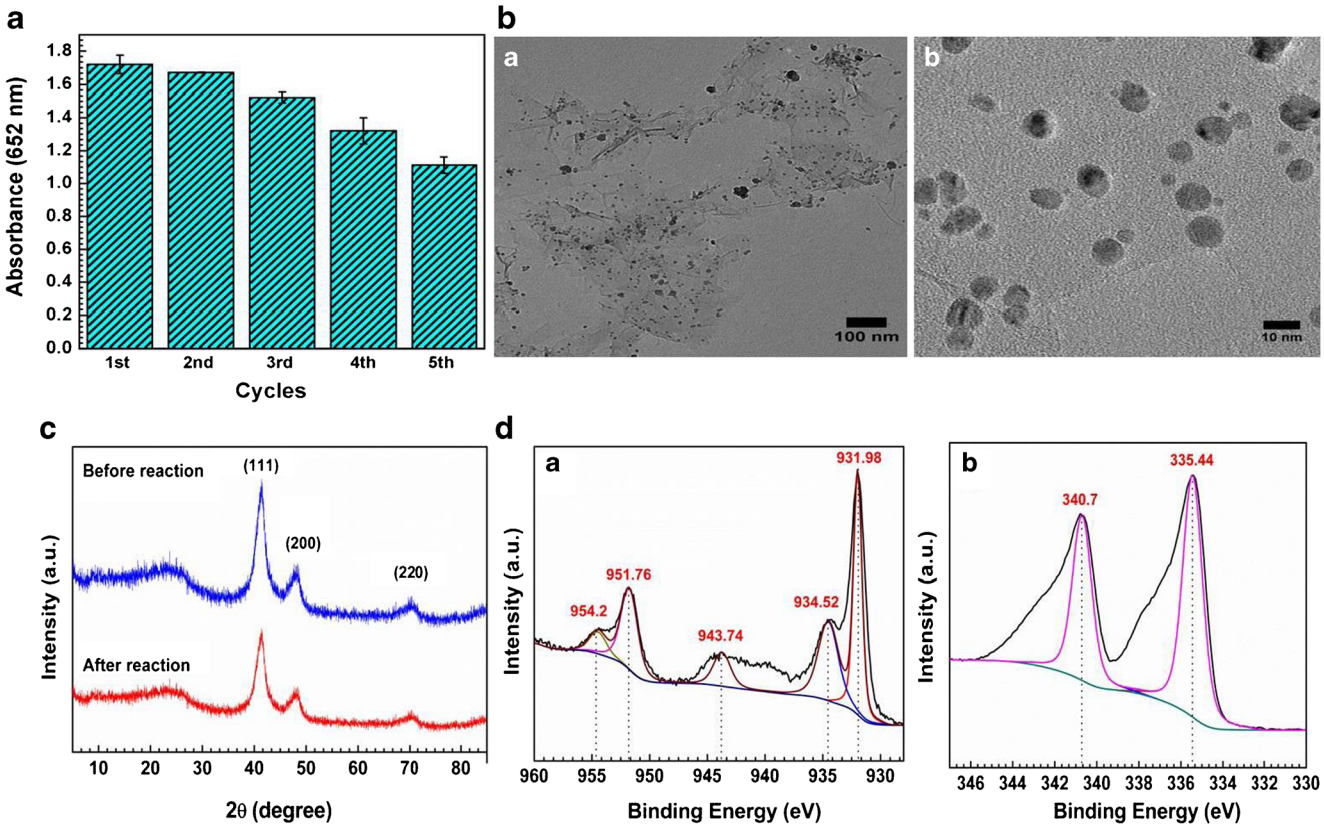

Fig. 6 **a** Recyclability of the Cu-Pd/rGO nanocomposite; **b** TEM analysis (**c**) XRD patterns and (**d**) XPS spectra of Cu-Pd/rGO nanocomposites after reuse

decreases with every recycling experiment indicating decrease in the efficiency of the Cu-Pd/rGO nanocomposites. The reusability experiment clearly indicates the efficient use of Cu-Pd/rGO upto five cycles without much activity loss. The structural, crystalline and oxidation changes associated with the reused Cu-Pd/rGO were studied using TEM, XRD and XPS. The TEM images (Fig. 6b(a,b)) shows spherical nanoparticles of Cu-Pd on rGO ascertaining retention in the morphology after five cycles of catalytic experiments. The XRD (Fig. 6c) also showed no change in its crystallinity. However, the XPS analysis shows changes in the oxidation states of Cu. In the Cu2p high resolution spectra (Fig. 6d(a)), peaks at 931.98 and 951.76 eV are due to $Cu2p_{3/2}$ and $Cu2p_{1/2}$, respectively from metallic Cu^0 or Cu^+ (Cu_2O). Peaks at 934.52 and 954.2 eV are from Cu^{2+} due to $Cu2p_{3/2}$ and $Cu2p_{1/2}$, respectively, arising from $Cu(OH)_2$ rather than CuO. The XPS analysis thus clearly indicated change in the oxidation state of Cu after continuous reuse. For Pd (Fig. 6d(b)), peaks at 335.4 and 340.7 eV corresponding to Pd $3d_{5/2}$ and Pd $3d_{3/2}$ respectively of bulk Pd(0) appear thus confirming no change in the oxidation of Pd after reuse.

Thus, Cu-Pd/rGO nanocomposites could be used to design a biosensor for precise determination of glucose in real and standard samples. The designed biosensor is reusable and sustainable in nature and can therefore be used for practical applications. Although a paper based analytical device using our nanozyme was constructed for the detection of standard glucose samples with encouraging results, yet this work has to be further extended to tests its applicability in real samples along with storage stability test for potential clinical applications.

Conclusion

The present work provides a chemical route for synthesizing bimetallic alloy Cu-Pd nanoparticles on rGO, g-C_3N_4 and MoS_2 nanosheets to form Cu-Pd/rGO, Cu-Pd/g-C_3N_4 and Cu-Pd/MoS_2 nanocomposites, respectively with an average size <10 nm. Amongst the 2D supports, rGO proved the best for obtaining Cu-Pd nanoparticles with controlled shape, size, crystallinity and oxidation state. All the Cu-Pd nanocomposites possessed intrinsic peroxidase like activity capable of catalyzing the oxidation of TMB, ABTS and OPD in presence of H_2O_2. The Cu-Pd/rGO nanocomposites demonstrated the best enzyme mimetic activity like peroxidase and oxidase than Cu-Pd/g-C_3N_4 and Cu-Pd/MoS_2 nanocomposites. Using rGO as scaffold, a novel enzymatic glucose sensor was constructed based on Cu-Pd nanoparticles which is sensitive, selective and can detect glucose with a low detection limit. The designed biosensor can also effectively determine glucose in serum samples. Further, it provided a base for the construction of a less costly paper based analytical device which is an alternating technique for glucose detection in practical fields. The designed biosensor can be reused upto five cycles and is sustainable in nature. Further research in this area may offer futuristic route towards developing other such nanomaterials based nanozymes for advanced applications in the area of biochemistry and biotechnology.

Acknowledgements Authors thank the Director, CSIR−NEIST, Jorhat. GD acknowledges DST, India for DST-INSPIRE Fellowship (GAP–0726). The authors acknowledges clinical center, CSIR-NEIST for providing the serum samples.

Compliance with ethical standards The author(s) declare that they have no competing interests.

References

1. Long YJ, Li YF, Liu Y, Zheng JJ, Tang J, Huang CZ (2011) Visual observation of the mercury-stimulated peroxidase mimetic activity of gold nanoparticles. Chem Commun 47:11939–11941
2. Natalio F, Andre R, Hartog AF, Stoll B, Jochum KP, Wever R, Tremel W (2012) Vanadium pentoxide nanoparticles mimic vanadium Haloperoxidases and thwart biofilm formation. Nat Nanotechnol 7:530–535
3. Mu J, Wang Y, Zhao M, Zhang L (2012) Intrinsic peroxidase-like activity and catalase-like activity of Co_3O_4 nanoparticles. Chem Commun 48:2540–2542
4. Shi W, Wang Q, Long Y, Cheng Z, Chen S, Zheng H, Huang Y (2011) Carbon Nanodots as peroxidase mimetics and their applications to glucose detection. Chem Commun 47:6695–6697
5. Yang J, Deng S, Lei J, Ju H, Gunasekaran S (2011) Electrochemical synthesis of reduced graphene sheet–AuPd alloy nanoparticle composites for enzymatic biosensing. Biosens Bioelectron 29:159–166
6. Yang L, Liu X, Lu Q, Huang N, Liu M, Zhang Y, Yao S (2016) Catalytic and peroxidase-like activity of carbon based-AuPd bimetallic nanocomposite produced using carbon dots as the reductant. Anal Chim Acta 930:23–30
7. Sun Z, Zhao Q, Zhang G, Li Y, Zhang G, Zhang F, Fan X (2015) Exfoliated MoS_2 supported Au–Pd bimetallic nanoparticles with core–shell structures and superior peroxidase-like activities. RSC Adv 5:10352–10357
8. Cai S, Han Q, Qi C, Lian Z, Jia X, Yang R, Wang C (2016) $Pt_{74}Ag_{26}$ nanoparticle-decorated ultrathin MoS_2 nanosheets as novel peroxidase mimics for highly selective colorimetric detection of H_2O_2 and glucose. Nanoscale 8:3685–3693
9. Wang M, Zhang W, Wang J, Wexler D, Poynton SD, Slade RCT, Liu H, Winther-Jensen B, Kerr R, Shi D, Chen J (2013) PdNi hollow nanoparticles for improved Electrocatalytic oxygen reduction in alkaline environments. ACS Appl Mater Interf 5:12708–12715
10. Kalidindi SB, Jagirdar BR (2012) Nanocatalysis and prospects of green chemistry. ChemSusChem 5:65–75
11. Guo S, Wang E (2011) Noble metal nanomaterials: controllable synthesis and application in fuel cells and analytical sensors. Nano Today 6:240–264
12. Quarta A, Corato RD, Manna L, Argentiere S, Cingolani R, Barbarella G, Pellegrino T (2008) Multifunctional nanostructures

based on inorganic nanoparticles and oligothiophenes and their exploitation for cellular studies. J Am Chem Soc 130:10545–10555
13. Shan S, Petkov V, Prasai B, Wu JF, Joseph P, Skeete Z, Kim E, Mott D, Malis O, Luo J, Zhong CJ (2015) Catalytic activity of bimetallic catalysts highly sensitive to the atomic composition and phase structure at the nanoscale. Nanoscale 7:18936–18948
14. Loukrakpam R, Shan SY, Petkov V, Yang LF, Luo J, Zhong CJ (2013) Atomic ordering enhanced Electrocatalytic activity of Nanoalloys for oxygen reduction reaction. J Phys Chem C 117: 20715–20721
15. Saikia H, Borah BJ, Yamada Y, Bharali P (2017) Enhanced catalytic activity of CuPd alloy nanoparticles towards reduction of nitroaromatics and hexavalent chromium. J Colloid Int Sci 486:46–57
16. Novoselov KS, Geim AK, Morozov SV, Jiang D, Zhang Y, Dubonos SV, Grigorieva IV, Firsov AA (2004) Electric field effect in atomically thin carbon films. Science 306:666–669
17. Wang R, Wu Z, Chen C, Qin Z, Zhu H, Wang G, Wang H, Wu C, Dong W, Fan W, Wang J (2013) Graphene-supported Au–Pd bimetallic nanoparticles with excellent catalytic performance in selective oxidation of methanol to methyl formate. Chem Commun 49:8250–8252
18. Zhang J, Chen Y, Wang X (2015) Two-dimensional covalent carbon nitride Nanosheets: synthesis, functionalization, and applications. Energy Environ Sci 8:3092–3108
19. Lv R, Robinson JA, Schaak RE, Sun D, Sun Y, Mallouk TE, Terrones M (2015) Transition metal Dichalcogenides and beyond: synthesis, properties, and applications of single- and few-layer Nanosheets. Acc Chem Res 48:56–64
20. Wang X, Blechert S, Antonietti M (2012) Polymeric graphitic carbon nitride for heterogeneous Photocatalysis. ACS Catal 2:1596–1606
21. Cheng Z, He B, Zhou L (2015) A general one-step approach for in situ decoration of MoS_2 nanosheets with inorganic nanoparticles. J Mater Chem A 3:1042–1048
22. Yang M, Ko S, Im J, Choi B (2015) Free-standing molybdenum disulfide/graphene composite paper as a binder- and carbon-free anode for lithium-ion batteries. J Power Sources 228:76–81
23. Jv Y, Li B, Cao R (2010) Positively-charged gold nanoparticles as peroxidase mimic and their application in hydrogen peroxide and glucose detection. Chem Commun 46:8017–8019
24. Kannel WB, McGee DL (1979) Diabetes and glucose tolerance as risk factors for cardiovascular disease: the Framingham study. Diabetes Care 2:120–126
25. Arun RK, Halder S, Chanda N, Chakraborty S (2014) A paper based self-pumping and self-breathing fuel cell using pencil stroked graphite electrodes. Lab Chip 14:1661–1664
26. Hummers WS, Offerman RE (1958) Preparation of graphitic oxide. J Am Chem Soc 80:1339–1339
27. Wu GW, Shen YM, Shi XQ, Deng HH, Zheng XQ, Peng HP, Liu AL, Xia XH, Chen W (2017) Bimetallic Bi/Pt peroxidase mimic and its bioanalytical applications. Anal Chim Acta 971:88–96
28. Yuan F, Zhao H, Zang H, Ye F, Quan X (2016) Three-dimensional graphene supported bimetallic nanocomposites with DNA regulated-flexibly switchable peroxidase-like activity. ACS Appl Mater & Interf 8:9855–9864
29. Vinita, Nirala NR, Prakash R (2018) A nanoporous palladium(II) bridged coordination polymer acting as a peroxidase mimic in a method for visual detection of glucose in tear and saliva. Microchim Acta 185:245–255
30. Tran HV, Nguyen TV, Nguyen ND, Piro B, Huynh CD (2018) A nanocomposite prepared from FeOOH and N-doped carbon nanosheets as a peroxidase mimic, and its application to enzymatic sensing of glucose in human urine. Microchim Acta 185: 270–280
31. Ishibashi K, Fujishima A, Watanabe T, Hashimoto K (2000) Quantum yields of active oxidative species formed on TiO_2 photocatalyst. J Photochem Photobiol A 134:139–142